# Motion Deblurring of RAW Mosaic Image using Coded Exposure Photography

Jaelin Lee and Byeungwoo Jeon
*Department of Electrical and Computer Engineering, Sungkyunkwan University, Suwon, Korea*
Jaelin@skku.edu, bjeon@skku.edu

***Abstract*—In this paper, a new motion deblurring method is investigated for reconstructing a latent image from a raw mosaic image that has been blurred by motion. Since conventional motion deblurring methods for color images often suffer from significant errors due to non-linear processing in color image processing pipeline, we devise a new deblurring technique by generating an invertible point spread function for deblurring of raw mosaic image by using coded exposure photography. The effectiveness of this method is demonstrated using a real dataset.**

***Keywords— Raw mosaic image deblurring, motion deblurring, coded exposure photography, image signal pipeline.***

## I. INTRODUCTION

Recovering a clear image from a motion-blurred one has been a longstanding challenge in the field of image processing and computer vision [1-4]. The blurring process is modeled as a convolution of the original sharp image, denoted by $m$, with a point spread function (PSF) $h$ that represents the blurring by the motion between camera and scene as follows:

$$i = h * m + \eta, \tag{1}$$

where $i$ is a blurred image, $*$ is the convolution operator, and $\eta$ is image noise. The model in (1) may hold properly for monochrome images, but we note not quite so for those color images captured by a digital color camera employing color filter array (CFA) due to its non-linear processing in image signal processor (ISP) [5, 6]. The imaging sensor in many digital color cameras is covered by an array of color filters, typically arranged in a Bayer pattern [6], which lets the sensor capture a selected color component only (for example, one out of R, G, B) at each pixel location. A full-color image having all three-color components at each pixel location is generated by a demosaicking processing in ISP which typically involves a series of non-linear processing [6, 7]. The full-color color image after ISP, denoted by $b$, is given as:

$$b = f(B(s * h) + \eta), \tag{2}$$

where $f$ models whole processing happening in ISP [5-7], $B$ represents image-sensing by color filter array (CFA) that generates a raw mosaic image [6], $s$ represents the latent image irradiance to the sensor, and $\eta$ is noise. Several kinds of non-linear processing [6-9] are inclusively represented by the function $f$ which can lead to performance degradation in color image deblurring [10]. One well-known such a non-linear processing is the demosaicking that interpolates the uncaptured color values at each pixel out by using those at neighboring pixels [7]. Lack of proper consideration in image deblurring [11] later regarding the undesirable artifacts generated by the demosaicking has put some limit on the performance of motion deblurring [12]. Another representative non-linear processing in ISP is a gamma correction (GC), which causes PSF estimation for motion deblurring not to be perfectly accurate [10].

One effective mitigation of those issues in ISP is to deblur a raw image before demosaicking. However, it should carefully consider that the latent raw mosaic image $B(s)$ cannot be simply convoluted as in (2) with the PSF $h$ due to the alternating under-sampling grid of the CFA pattern, e.g., Bayer pattern array [6]. For this reason, some recent works have estimated the latent images from the demosaicked color image under several assumptions to make the deblurring methods more realistic, *e.g.*, by employing dark channel prior [13] or local minimal intensity prior [14]. To make the deblurring performance even better, [15] has employed a deep learning-based denoiser prior, a kernel error term, and a residual error term. In [16], post-processing has been applied to the dataset to reduce the domain gap between raw image and color image, but the averaged RGB dataset captured by a high-speed camera still cannot simulate the real-world blur well due to the ISP. Novel methods for improving PSF invertibility in photography have been proposed, including parabolic camera motion in [17] and phase encoding combined with machine learning-based deblurring algorithms in [18]. To deblur the raw mosaic image, subsampling algorithm have been used in previous works. For example, in [19], the latent image was iteratively reconstructed from color-subsampled raw sensor data. In [20], a machine-learning-based approach was also proposed to reconstruct the sharp color image from the color-subsampled raw mosaic image. However, since the relationship between the latent image of the color-subsampled image and the PSF is still not a simple convolution relation as in (2), the deblurring inevitably suffers, which is modeled as much noise.

Our method in this paper is to modulate the relationship between PSF and raw mosaic image by employing a technique of coded exposure photography (CEP) [21-25]. The image is motion-blurred due to motion during camera shutter exposure which takes a rectangular pulse shape in the time domain. Since the Fourier transform of the rectangular pulse is the Sinc function with many zeros, this conventional exposure process behaves like a non-invertible filter thus losing spatial details in the deblurred image. To solve this, CEP modulates the light entering camera by adjusting the shutter exposure [21]. In this paper, we modulate the PSF considering the CFA pattern placed along the path of the point spread, *i.e.*, motion trajectory, to help restoring the latent image from the raw mosaic image. By employing our proposed method of motion deblurring on the raw mosaic image, we demonstrate better ability to obtain a sharp image than traditional CEP methods by mitigating noise arising in the ISP. We demonstrate the effectiveness of our method by experimenting with real data.

This work was supported in part by Basic Science Research Program (RS-2023-00208453) through the National Research Foundation of Korea (NRF) and by the ICT Creative Consilience Program (IITP-2023-2020-0-01821) supervised by the IITP(Institute for Information & communications Technology Planning & Evaluation), both funded by the Ministry of Science and ICT, Korea.

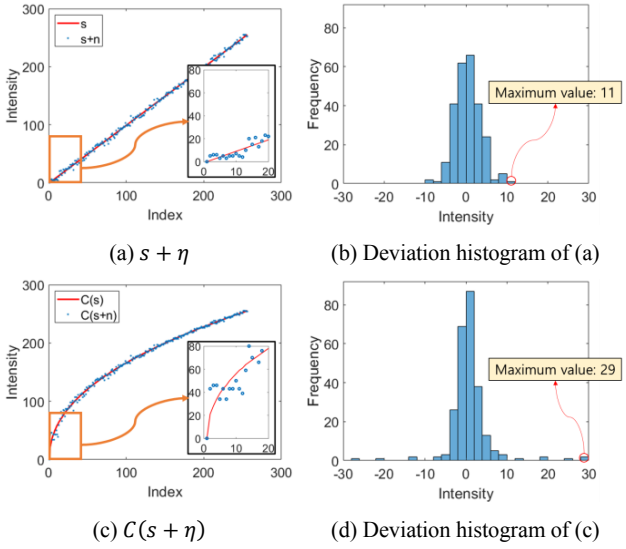


(a) $s+\eta$ (b) Deviation histogram of (a)

(c) $C(s+\eta)$ (d) Deviation histogram of (c)

Figure 1. Graphs and histograms showing noise amplification by gamma correction $C$. In (a) and (c), a red line is the noiseless signal, and a blue dot represents the signal with Gaussian noise $\mathcal{N}(0,3^2)$. In (c), the gamma $\gamma$ used for gamma correction is 2.2. (b) and (d) are histograms that visualize the deviations between the noiseless and the noisy signals of (a) and (c), respectively. The variances of (b) and (d) are 9.73 and 24.39, respectively.

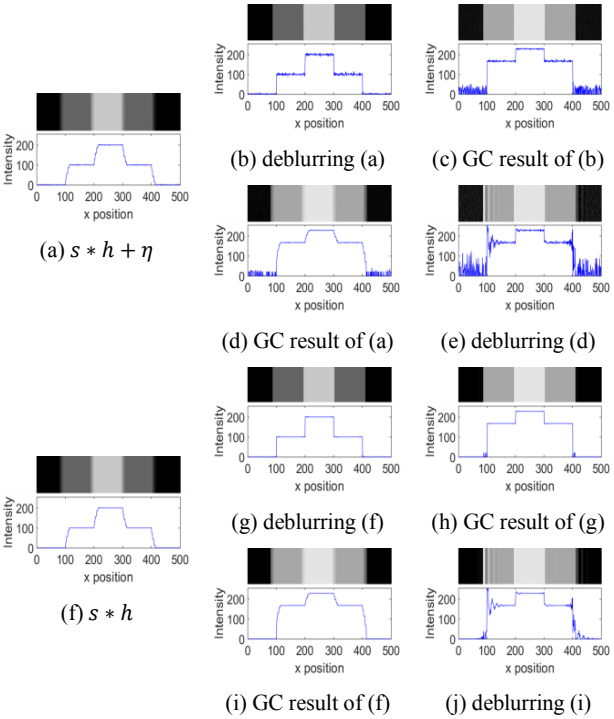


(a) $s*h+\eta$ (b) deblurring (a) (c) GC result of (b)

(d) GC result of (a) (e) deblurring (d)

(f) $s*h$ (g) deblurring (f) (h) GC result of (g)

(i) GC result of (f) (j) deblurring (i)

Figure 2. Comparison of motion deblurring results to analyze the effect of gamma correction (GC) on image deconvolution. The method in [4] is used for deblurring. Note that (a)-(e) are for illustrating noise amplification in noisy image deblurring, and (f)-(j) are for demonstrating the deconvolution error [10] in the noiseless image deblurring procedure.

## II. Artifacts of Image Deblurring Due to ISP

The deblurring artifacts due to non-linear processing in ISP is illustrated in Fig. 2 using synthetic data. To make our analysis more focused and illustrative, we employed a monochrome camera (that is, without CFA). The camera response function (CRF) [8], which describes relation between scene radiance and the captured image intensity, approximates the response of the whole system as a single function with all procedures inside [8]. Actual CRF curve is different individually for each camera, but most camera manufacturers design the CRF to be a gamma curve [8] due to the gamma correction (GC). We denote the GC by $C$ where $C(a)=a^{\gamma}$. As a consequence of applying GC, the maximum intensity and variance of noise increases as shown in Fig. 1. Thus, when deblurring a raw image, the noise in deblurred image $(\eta * h^{-1})$ is increased as shown in Fig. 2(c). Note that deblurring of the final gamma corrected image shows further amplified noise depending on the blur kernel as in Fig. 2(e).

One additional problem to note in association with applying GC is that it causes errors in motion deblurring and PSF estimation [10]. To focus on the analysis, we assume that the noise is negligible ($\eta \approx 0$). We can design the noiseless grayscale blurred image by considering GC as $C(s*h)$ as shown in Fig. 2(i), where $s$ is the latent image irradiance. Let us denote the difference between before and after applying GC as $\Gamma$, that is, $\Gamma = C(s*h)-(s*h)$. After the deblurring performed without proper consideration of the GC, the computed sharp image will be:

$$\hat{s} = C(s*h)*h^{-1}, \tag{3}$$

where $\hat{s}$ is a computed sharp image, and $h^{-1}$ is the inverse filter of $h$. Note that $C(s*h)=(s*h)+\Gamma$, (3) can be expressed as:

$$\hat{s} = s+(\Gamma*h^{-1}), \tag{4}$$

and $\Gamma*h^{-1}$ represents the additional deconvolution artifacts. As shown in Fig. 2(j), the deblurring result is confirmed not promising due to the additional deblurring noise.

## III. Raw Image Deblurring Using CEP

### A. CFA impact on raw image deblurring

Our goal is deblurring a raw image as defined in (5) to avoid the noise mentioned in the previous section.

$$r = B(s*h)+\eta \tag{5}$$

Since the CFA, denoted by $B$, filters the incident light for each photosensor independently according to the spectral sensitivity of its each color filter, the raw mosaic image cannot be processed using the PSF estimation and subsequent deconvolution modeled as (1) [4]. To obtain the latent raw mosaic image, which can be denoted as $B(s)$, we can design the following inverse filtering process:

$$B(\hat{s}) = B(B^{-1}(r)*h^{-1}), \tag{6}$$

where $B(\hat{s})$ is the computed latent raw mosaic image. Note that the intensity of the raw mosaic image is a result of integrated continuous signals filtered by CFA [9] as:

$$B(s)[n] = \int_{n-0.5}^{n+0.5}\int_{\lambda}\Phi(\lambda,x)l(\lambda,x)d\lambda\,dx, \tag{7}$$

where $n$ is the center position of the pixel, $\Phi$ represents the spectral response of CFA, $l$ denotes the relative intensity of the light, and $\lambda$ is the wavelength. Thus, inversion of $B$ is an ill-posed problem.

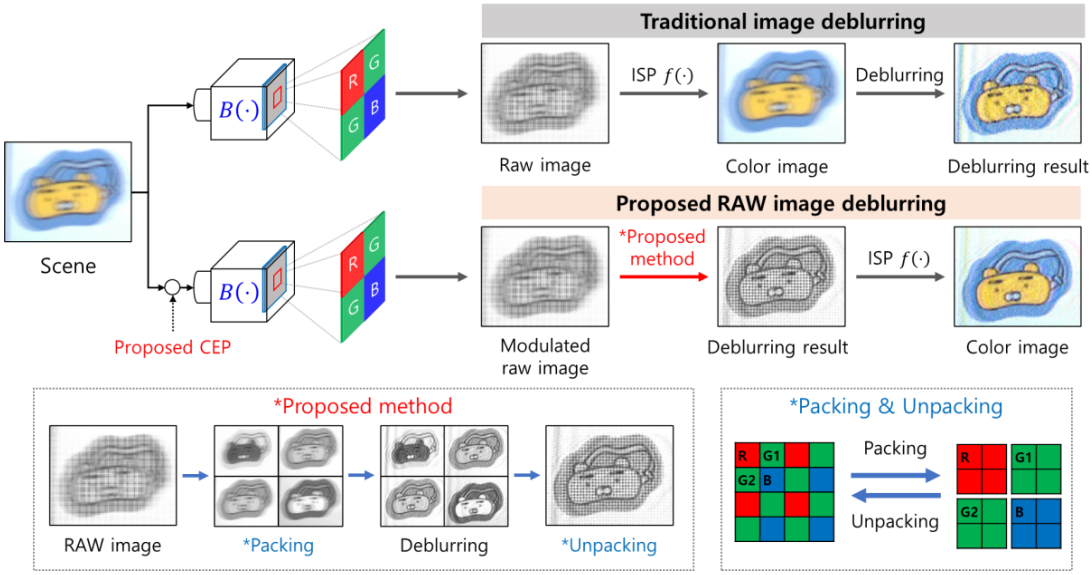


Figure 3. Comparison between conventional deblurring method and the proposed deblurring approach.

### B. *Proposed deblurring scheme of RAW mosaic image*

To better understand our method, let's assume the 1D uniform linear motion. The complex motions such as camera shake can be understood as a collection of 1D manifolds [21]. For 1D motion, the discrete equation of the blurred raw image in a vector form can be written as:

$$\mathrm{r}[n] = \sum_{k=0}^{K-1} B(\mathrm{s}[n-k]h[k]) + \eta[n], \tag{8}$$

where $\mathrm{r}, \mathrm{s}$, and $\eta$ denote the vectors of blurred raw image, latent image irradiance, and noise along each motion line, respectively. Since the inverse of $B$ cannot be simply computed in (8), the latent raw image $B(\hat{s})$ cannot be calculated directly.

The purpose of our method is to obtain an invertible PSF for raw mosaic image using CEP, and the key is to generate a code fully considering the CFA pattern. Such a code, denoted by $U$, can optimize the invertibility of PSF for a given motion, thus eventually helping the deconvolution process [21]. The raw image captured by CEP, $\mathrm{r}^{CEP}$ can be expressed as:

$$\mathrm{r}^{CEP}[n] = \sum_{k=0}^{K-1} B(\mathrm{s}[n-k]h[k]u[k]) + \eta[n], \tag{9}$$

where $u[k]$ is the $k^{th}$ element of the code $U$ with $U = \{u[0], u[1], \dots, u[K-1]\}$. Note that $B$ depends on the location $n$ due to the different spectral sensitivity of each color filter as in (7). For 1D motion, scene radiance is filtered by one row or column in the Bayer pattern array. Thus, we define $B_1$ and $B_2$ as the two different color filters that make up each row of the Bayer pattern array. If the $n^{th}$ pixel of the blurred image has been filtered by $B_1$, the relationship between the latent raw image $B(s)$ and the blurred image can be represented as follows:

$$\mathrm{r}^{CEP}[n] = \sum_{k=0}^{(K-1)/2} B_1\Big(\mathrm{s}[n-2k]h[2k]u[2k] + B_2^{-1}\big(B_2(\mathrm{s}[n-(2k+1)]h[2k+1]u[2k+1])\big)\Big) + \eta[n]. \tag{10}$$

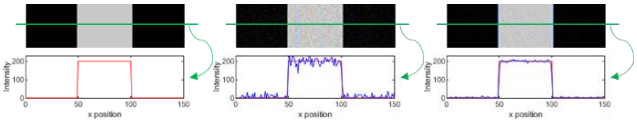

(a) Ground truth $s$ (b) Conventional CEP (c) Proposed method

Figure 4. Synthetic experiment result. (a) is an image irradiance $s$. We generate the blurred image with 1D motion and ISP functions [6]. (b) shows the result reconstructed by a conventional method [22], and (c) shows the deblurring result by the proposed method. Note that the optimization method for the code used in (b) and (c) are the same method of [22]. The graph below each image in (a) to (c) represent the signals of selected rows indicated by the green line.

Although we still cannot obtain the inverse of $B_2$, we can manipulate the code to remove the corresponding term. Here, we propose a code generation method of fixing $u[2k+1]$ to 0 as:

$$U = \{u[0], 0, u[2], 0, \dots, 0, u[K-2], 0\}. \tag{11}$$

Since $u[2k+1]$ is 0, the signal filtered by the color filter with $B_2$ is eliminated. Also, since the same color filter is located on the $\big(n-(2k+1)\big)^{th}$ pixel, we can rewrite (10) as:

$$\mathrm{r}^{CEP}[n] = \sum_{k=0}^{K-1/2} B_1(\mathrm{s}[n-k])h^{CEP}[k] + \eta[n], \tag{12}$$

where $h^{CEP}$ is a coded PSF and represents the element-wise multiplication of $h$ and $u$. (12) can be expressed as convolution relation between $B_1(s)$ and $h^{CEP}$:

$$\mathrm{r}^{CEP} = B_1(\mathrm{s}) * h^{CEP} + \eta. \tag{13}$$

Since the PSF of the $\mathrm{r}^{CEP}$ is designed to spread only with the same color filter $B_1$ as $n$, it can pack the same color pixels into one channel image and divide the raw image into four-channel (RGGB) images as shown in Fig. 3. Finally, we apply ISP functions to the reconstructed raw image to obtain a sharp color image as:

$$f\big(\widehat{B_1(\mathrm{s})}\big) = f(\mathrm{r}^{CEP} * (h^{CEP})^{-1}). \tag{13}$$

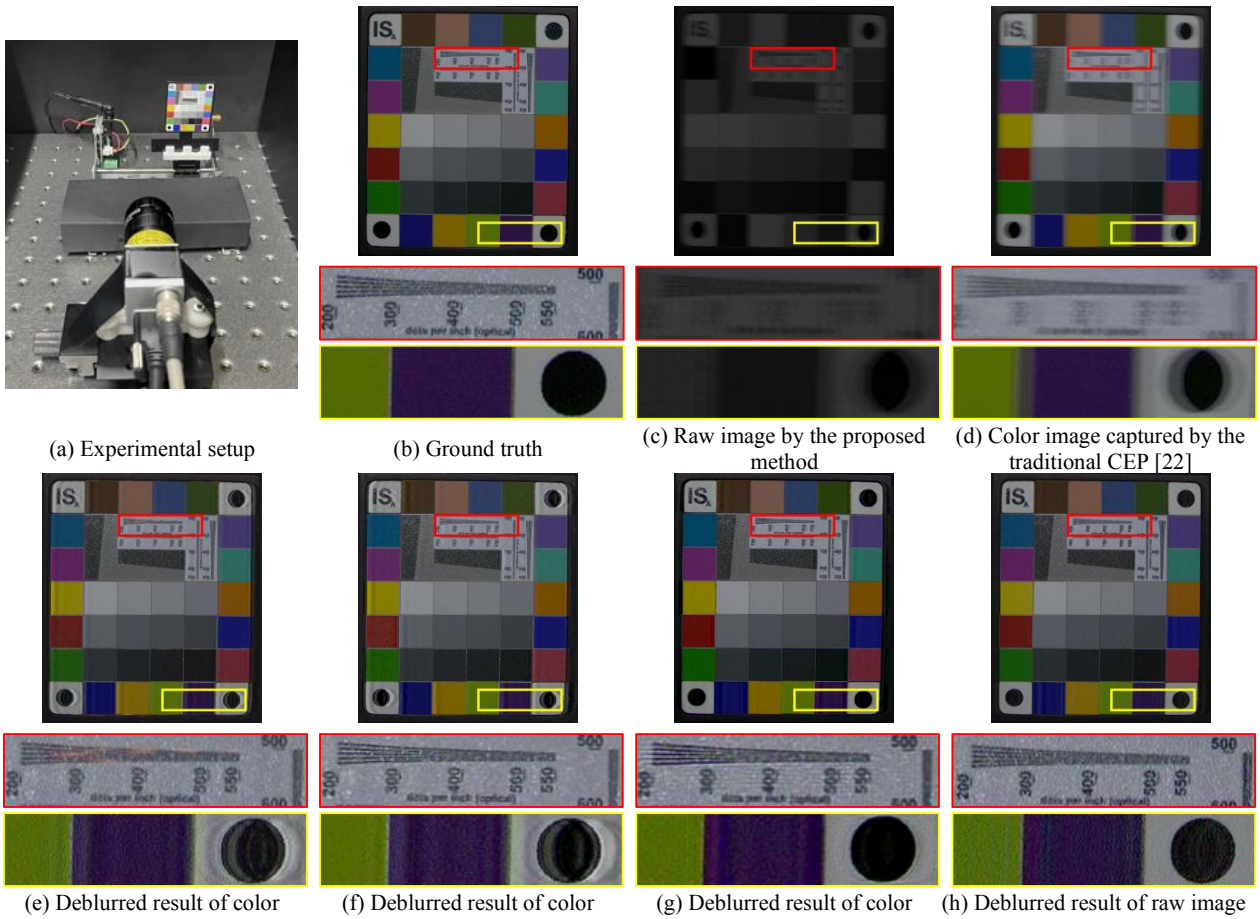

(a) Experimental setup (b) Ground truth (c) Raw image by the proposed method (d) Color image captured by the traditional CEP [22]

(e) Deblurred result of color image (d) by [22] (f) Deblurred result of color image (d) by [14] (g) Deblurred result of color image (d) by [15] (h) Deblurred result of raw image (c) by the proposed method

Figure 5. Experiment results. (a) Experimental setup, (b) captured stationary image as a ground truth, (c) raw image with motion blur, (d) color image reconstructed from (c) using white balancing, gamma correction [6] and demosaicking [26]. (e-g) are deblurring results of color image (d) by using [22], [14], [15], respectively. (h) is the deblurring result of raw image (c) by using the proposed method.

The code generated using the proposed method, which considers motion and CFA, is optimized using conventional optimization methods [21-23].

## IV. Experimental Result

We experimentally demonstrate the performance by using a synthetic and real data. For fair comparison, we use the code in our experiment that has the same performance as the code optimized by traditional method [22]. The code used in [22] is '1100000000000110000100101000001,' and the proposed code is '1010000010101010000000000100010.' The experiment using synthetic data uses the codes above is shown in Fig. 4, where Fig. 4(a) is the latent image irradiance, Fig. 4(b) shows the deblurring result from $f(B(s*h)+\eta)$, and Fig. 4(c) shows the deblurring result from $B(s*h^{CEP})+\eta$ and applying ISP after deblurring. Since CFA is a well-known spatially variant system [6], to simplify the experiment, it was conducted assuming a scene with two types of reflectance, as shown in Fig. 4(a). The noise is a random Gaussian noise with a mean of 0 and a standard deviation of 1. The PSNR (peak-to-noise-ratio) and SSIM (structure similarity) are used for objective evaluation, and [PSNR, SSIM] of Fig. 4(b) and (c) are [25.14(dB), 0.1863] and [36.40(dB), 0.6706], respectively. Although the invertibility of the coded PSFs used for deconvolution is the same, we confirmed that our proposed method increased PSNR by 11dB compared to the conventional method [22].

We captured a real scene as shown in Fig. 5 to demonstrate the effectiveness of our proposed method. The hardware setup for real experiment is shown in Fig. 5(a). To exclude the artifacts caused by PSF estimation in evaluating the proposed method, we control the motion so that the PSF is known in advance. For experiment, an object is mounted on a conveyor belt shown in Fig. 5(a) and we control its motion to move uniformly in 1D direction. Images of real moving objects are captured by the Basler acA2040 Bayer pattern CFA-based color camera [27]. We turned off all ISP options when capturing the raw mosaic image. To modulate the image using CEP, we carry out the experiment in a darkroom using a strobing LED synchronized with the camera. The codes used in the synthetic experiments are used for real experiments. We employ the CEP [22], dark channel prior [14], and local minimal intensity prior [13] for comparison. Note that the conventional deblurring methods are applied to the color image in Fig. 5(d). This is almost identical to the outcome obtained by converting the raw image in Fig. 5(c) into a color image using ISP and then applying deblurring to it, because the performance of the codes used in Fig. 5(c) and Fig. 5(d) are the same.

The acquired raw image is shown in Fig. 5(c), and the color image produced from the raw image using ISP [6] with demosaicking [26] is shown in Fig. 5(d). Our proposed method is applied to Fig. 5(c), and the result is shown in Fig. 5(h). Prior arts for comparison are color image deblurring

methods, so these are applied to Fig. 5(d), and the results are shown in Fig. 5(e-g). In those results reconstructed by traditional methods [14, 15, 22], the deconvolution noises, *e.g.*, ringing artifact and zippering artifact, are found due to non-linear functions in ISP. Our proposed method, a novel attempt for deconvolution on raw mosaic images, is seen to reduce the deconvolution noises significantly compared to the prior arts as shown in Fig. 5(h).

In both experiments with synthetic and real data, we confirm improved performance of the proposed method compared to the prior arts. This is because our proposed method successfully acquires an invertible PSF for raw mosaic image, so that it is not affected by ISP noise while reconstructing latent raw mosaic image.

## V. Conclusion

In this paper, we proposed a novel scheme that reconstructs a latent image after deblurring raw mosaic image. Inspired by CEP [21], our proposed method modulates the raw mosaic image to prevent deblurring artifacts caused by ISP. By deblurring raw image, we can significantly remove the deconvolution artifacts caused by ISP. We confirmed the effectiveness of our proposed method through an experiment using a real dataset. Since our proposed method is a PSF modulating method in consideration of the CFA, it can be extended to various CFA formats and can be applied to cutting-edge CEP methods for optimizing the code [28, 29].

One limitation of our work is that we only solve for a given motion like other CEP methods [21-23]. Although many real motions, *e.g.*, moving cars on the highway or flow cytometry, result in predictable motion as mentioned in [32], the proposed technique may be difficult to apply to problems under general environments due to its constraints. In the future, as motion observation technology advances, it may be possible to extend the application of the proposed technique to more general environments. Unique code generation for more general PSF will be also a promising direction of research in the future.

## References


[1] L. B. Lucy, "An iterative technique for the rectification of observed distributions," in Astronomical Journal Papers, vol. 79, no. 7, pp. 745–754, 1974.

[2] W. H. Richardson, "Bayesian-based iterative method of image restoration," in Journal of the Optical Society of America, vol. 62, no. 1, pp. 55–59, 1972.

[3] N. Wiener, Extrapolation, Interpolation, and Smoothing of Stationary Time Series: With Engineering Applications, The MIT Press Publishers, Massachusetts, pp. 81-112, 1964.

[4] A. Levin, Y. Weiss, F. Durand, and W. T. Freeman, "Understanding and evaluating blind deconvolution algorithms," in Proc. IEEE Conf. on Computer Vision and Pattern Recognition, 2009, pp. 1964–1971.

[5] G. Sharma and H.J. Trussell, "Digital color imaging," in IEEE Trans. on Image Processing, vol. 6, no. 7, pp. 901-932, 1997

[6] R. Ramanath, W. E. Snyder, Y. Yoo, and M. S. Drew, "Color image processing pipeline," in IEEE Signal processing magazine, vol. 22, no. 1, pp. 34-43, 2005.

[7] B. K. Gunturk, J. Glotzbach, Y. Altunbasak, R. W. Schafer, and R. M. Mersereau, "Demosaicking: color filter array interpolation," in IEEE Signal Processing Magazine, vol. 22, no. 1, pp. 44-54, 2005.

[8] M. D. Grossberg, and S. K. Nayar, "Modeling the space of camera response functions," in IEEE Trans. on Pattern Analysis and Machine Intelligence, vol. 26, no. 10, pp. 1272-1282, 2004.

[9] S. Lin, and L. Zhang, "Determining the radiometric response function from a single grayscale image," in Proc. IEEE Conf. on Computer Vision and Pattern Recognition, 2005, pp. 63-73.

[10] Y. W. Tai, X. Chen, S, Kim, S. Kim, F. Li, J. Yang, Y. Matsushita, and M. S. Brown. "Nonlinear camera response functions and image deblurring: theoretical analysis and practice," in IEEE Trans. on Pattern Analysis and Machine Intelligence, vol. 35, no. 10, pp. 2498-2512, 2013.

[11] P. A. Jansson, Deconvolution of Images and Spectra, Academic press, 2nd edition, 1997.

[12] S. Har-Noy, S. H. Chan, and T. Q. Nguyen, "Demosakcing images with motion blur," in Proc. IEEE Int. Conf. of Acoustic, Speech and Signal Processing, 2010, pp. III-485 - III-488.

[13] J. Pan, D. Sun, H. Pfister, and M. H. Yang. "Deblurring images via dark channel prior," in IEEE Trans. on Pattern Analysis and Machine Intelligence, vol. 40, no.10, pp. 2315–2328, 2018.

[14] F. Wen, R. Ying, Y. Liu, P. Liu, and T.K. Truong, "A Simple Local Minimal Intensity Prior and an Improved Algorithm for Blind Image Deblurring," in IEEE Trans. on Circuits and Systems for Video Technology, vol. 31, no. 8, pp. 2923-2937, 2020.

[15] Y. Fang, H. Zhang, H. Wong and T. Zeng, "A Robust Non-Blind Deblurring Method Using Deep Denoiser Prior," in Proc. IEEE Conf. on Computer Vision and Pattern Recognition, 2022, pp. 735–744.

[16] S. Nah, T. H. Kim, and K. M. Lee, "Deep multi-scale convolutional neural network for dynamic scene deblurring," in Proc. IEEE Conf. on Computer Vision and Pattern Recognition, 2017, pp. 3883-3891.

[17] A. Levin, P. Sand, T. Cho, F. Durand and W. T. Freeman, "Motion-invariant photography." ACM Trans. On. Graphics (TOG), vol. 27, no. 3, pp. 1-9, 2008.

[18] S. Elmalem, R. Giryes and E. Marom, "Motion deblurring using spatiotemporal phase aperture coding." Optica, vol. 7, no. 10, pp. 1332-1340, 2020.

[19] M. Trimeche, D. Paliy, M. Vehvilainen, and V. katkovnik, "Multichannel image deblurring of raw color components," in Computational imaging III, vol. 5674, pp. 169-178, 2005.

[20] C. H. Liang, Y. A, Chen, Y. C. Lie, and W. H. Hsu, "Raw image deblurring," in IEEE Trans. On Multimedia, vol. 24, pp. 61-72, 2020.

[21] R. Raskar, A. Agrawal, and J. Tumblin, "Coded exposure photography: motion deblurring using fluttered Shutter," in ACM Trans. on Graphics, vol. 25, no. 3, pp. 795-804, 2006.

[22] A. Agrawal, and R. Raskar, "Optimal single image capture for motion deblurring," in Proc. IEEE Conf. on Computer Vision and Pattern Recognition, 2009, pp. 2560-2567.

[23] S. McCloskey, Y. Ding, and J. Yu, "Design and estimation of coded exposure point spread functions," in IEEE Trans. on Pattern Analysis and Machine Intelligence, vol. 34, no. 10, pp. 2071-2077, 2012.

[24] S. McCloskey, "Temporally Coded Flash Illumination for Motion Deblurring", International Conf. on Comput. Vis., 2011.

[25] C. Ma, Z. Liu, L. Tian, Q. Dai, and L. Waller, "Motion deblurring with temporally coded illumination in an LED array microscope," Opt. Lett.,vol. 40, no. 10, pp. 2281-2284, 2015.

[26] S. M. Henrique, L. He, and R. Cutler, "High quality linear interpolation for demosaicing of Bayer-patterned color images," in Proc. IEEE Int. Conf. of Acoustic, Speech and Signal Processing, 2004, pp. III-485 - III-488.

[27] P. M. Hubel, J. Liu, and R. J. Guttosch. "Spatial frequency response of color image sensors: bayer color filters and foveon X3," in Sensors and Camera Systems for Scientific, Industrial, and Digital Photography Applications V. Vol. 5301. International Society for Optics and Photonics, 2004.

[28] Z. Wang, A. C. Bovik, H. R. Sheikh, and E. P. Simoncelli, "Image quality assessment: From error visibility to structural similarity," in IEEE Trans. Image Processing, vol. 13, no. 4, pp. 600–612, 2004.

[29] "Basler Camera". https://www.baslerweb.com/en/products/cameras/area-scan-cameras/ace/aca2040-120uc/ (20 November 2020).

[30] H.G. Jeon, J.Y. Lee, Y. Han, S.J. Kim, and I.S. Kweon, " Multi-Image Deblurring Using Complementary Sets of Fluttering Patterns," in IEEE Trans. on Image Processing, vol 26, no. 5, pp. 2311-2326, 2017.

[31] C. Tsutake and T. Yoshida, "Reduction of Poisson Noise in Coded Exposure Photography," in Proc. IEEE International Conf. on Image Processing, 2018, pp. 3938-3942.

[32] S. McCloskey, "Velocity-Dependent Shutter Sequences for Motion Deblurring," in European Conference on Computer Vision, 2010, pp. 309-32